Calibrated Cosmic Muon Simulations for the HCal

Hanpu Jiang, Shuhang Li*, Emma McLaughlin, Blair Seidlitz, Bill Zajc

August 2022

1 Introduction

The main purpose of this study is to develop a cosmic muon generator with realistic zenith angle and energy distribution to investigate the possibility of using cosmic muon events as a calibration source for the hadronic calorimeters (HCal's) when the full sPHENIX apparatus is in its data-taking position. Comparisons of simulations using the generator to measured cosmic muon ADC distributions taken in Building 912 with the test stand electronics show good agreement. This note also describes an independent derivation from the LED data of the simulation parameter `m_photonelecADC` $\equiv$ the number of photoelectrons per ADC count.

2 Cosmic Muon Generator

The cosmic muon generator that was used in this study works as a wrapper class of the open source cosmic muon generator EcoMug [1]. The muons are generated on the surface of a half-sphere with radius of 6.5 meters covering the entire sPHENIX detector, making it suitable for studies for all of the sPHENIX sub-systems.

2.1 Simulation Setup

All of the simulations were conducted using the sPHENIX Fun4All framework. In these initial GEANT4 simulations, only the outer HCal(OHCal), inner HCal(IHCal), and the magnet was built, the boundary of the simulation is extended(by setting Enable::BLACKHOLE option false in the Fun4All macro) enabling all muons to reach the detector. The truth information of the generated muons as well as energy deposition in HCal towers was written in a TTree. (This study was done with the sPHENIX weekly build ana 295, however, for new studies, using newer builds when the cosmic muon generator is added in to the main repository is recommended.)

In the digitization process of the simulation, `tower_sim` = the sum of energy in the active volume for each tower is converted to `tower_raw` = digitized ADC value with Poisson fluctuations on the inferred number of photoelectrons, then the ADC value is converted to `tower_calib` = the total energy loss in tower. On average, 1 ADC $\approx$ 0.2 MeV for OHCal, 0.4 MeV for IHCal visible scintillator energy deposition, which after division by the OHCal sampling fraction f_{Outer} = 0.0338 becomes 1 ADC $\approx$ 5.916 MeV total energy loss. For IHCal 1 ADC $\approx$ 2.466 MeV total energy loss[1].

2.2 Comparison to Test Stand Data

When the detector is in the assembled position, two rows of towers with ϕ index 0 and 1 have the same orientation as the outer HCal sectors during the cosmic testing in Building 912. Therefore, applying the same cuts that were used in the OHCal cosmic testing and comparing the energy distribution is a good test for the validity of the cosmic muon generator as well as the GEANT4 simulation. After applying the vertical cut (requiring the tower above to have no less than 5 MeV in the active volume),

---

*Corresponding author: sl4859@columbia.edu

[1]We have attempted to document the provenance of these factors in the Appendix

and the veto cut (requiring that none of the adjacent towers have energy greater than 1.2 MeV in the active volume), the simulated energy distribution shape of the selected towers agreed very well with the test stand result, as shown in Figure 1. However, there are some disagreement in the absolute energy scale, the truth energy deposition in figure 1 peak at 7 MeV, base on the simulation constant shown in the Appendix, correspond to 560 ADC in high gain mode, while the test stand MPV is at 350 ADC which is about 63% of the simulated value.
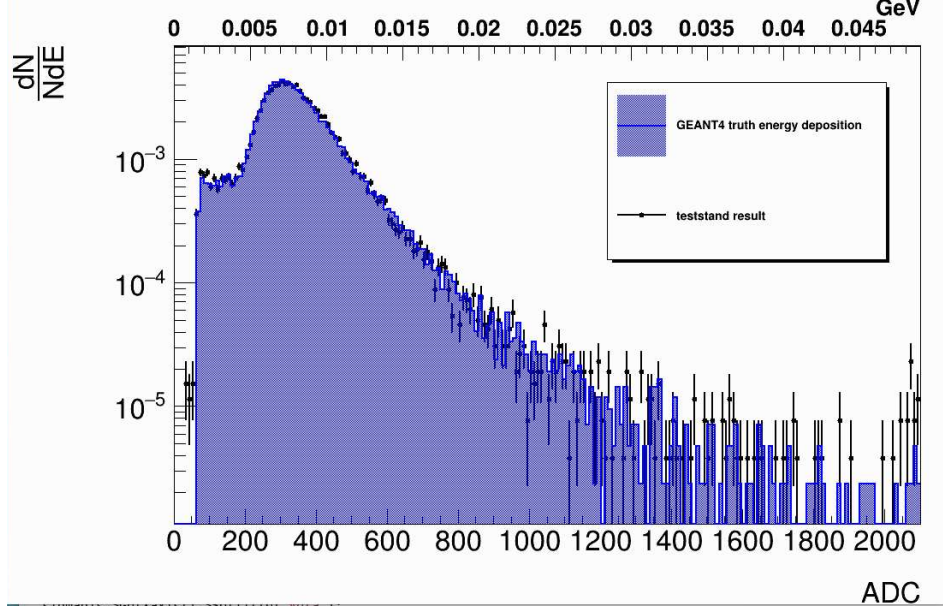

Figure 1: The simulated truth energy distribution(in GeV) and the cosmic test stand result (in ADC) for OHCal. The two distributions have very similar shapes.

2.3 Comparison to Calibrations Derived from the LED Data

Two parameters are used in the simulations to map the energy deposited in the scintillator E_{dep}^{scint} to the ADC scale: the number of photoelectrons in the SiPM per GeV energy deposited in the scintillator, and the number of ADC counts per photoelectron. While the mapping from the GEANT-determined E_{dep}^{scint} to ADC counts is the product of these two factors, determining the number of photoelectrons as an intermediary is necessary in order to incorporate the Poisson fluctuations on this number.

We have determined that is is possible to extract an estimate for this second factor $S \equiv$ the number of ADC counts per photoelectron from the LED data. Figure 2 shows a typical ADC distribution for a tower when pulsed by the LED system. If we assume a strictly linear response between the LED output and the ADC value proportional to the number of photoelectrons N_{pe}, and that there are no fluctuations in the LED output, then the ADC distribution should determined by the Poisson[2] fluctuations in N_{pe}. Under these assumptions, the scale factor S is determined from the MPV and relative rms width w of the distribution

$$MPV = S \cdot N_{pe} \quad \oplus \quad w = \frac{1}{\sqrt{N_{pe}}} \quad \Rightarrow \quad S = w^2 MPV \quad .$$

A potential criticism of this procedure is that it ignores the contribution to the width of the LED distribution due to fluctuations in the LED output. Assuming that the relative fluctuations contribute in quadrature the measured width $w_{measured}^2 = w_{truth}^2 + \Delta_{LED}^2$, where we denote the purely Poisson width called w above as w_{truth}. We then have

$$w_{measured}^2 = w_{truth}^2 + \Delta_{LED}^2 = \frac{S_{truth}}{MPV} + \Delta_{LED}^2 = \frac{S_{measured}}{MPV} \Rightarrow S_{measured} = S_{truth} + \Delta_{LED}^2 \cdot MPV \quad ,$$

---

[2]For any reasonable number of mean photoelectrons $> \sim 30$ the Poisson is indistinguishable from a Gaussian
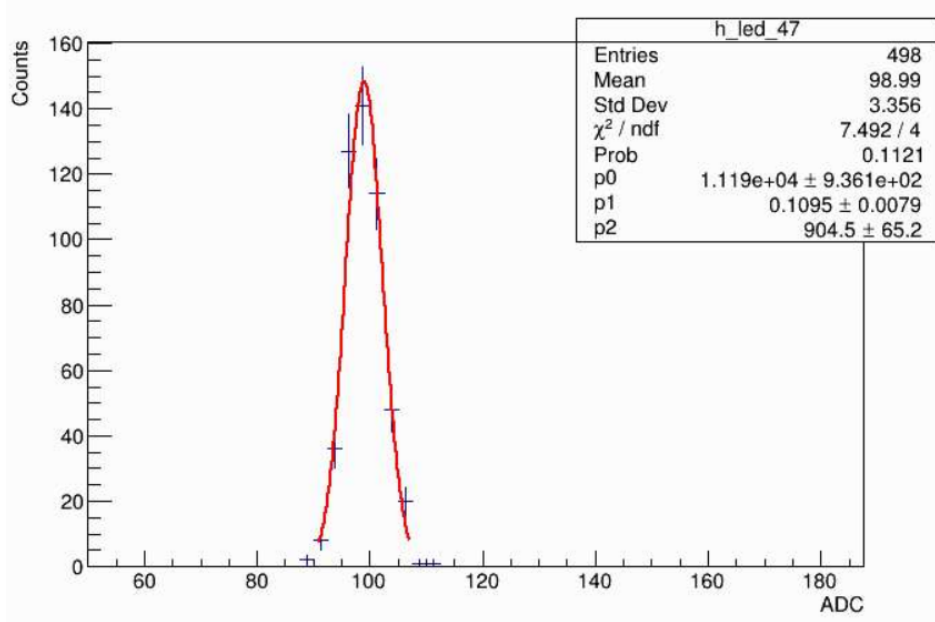
Figure 2: A typical ADC distribution from the LED pulser for the IHCal (Sector 19, Tower #47) fit with a Poisson distribution. Parameter 1 is the scale factor determined by the fit; parameter 2 is the number of photoelectrons.
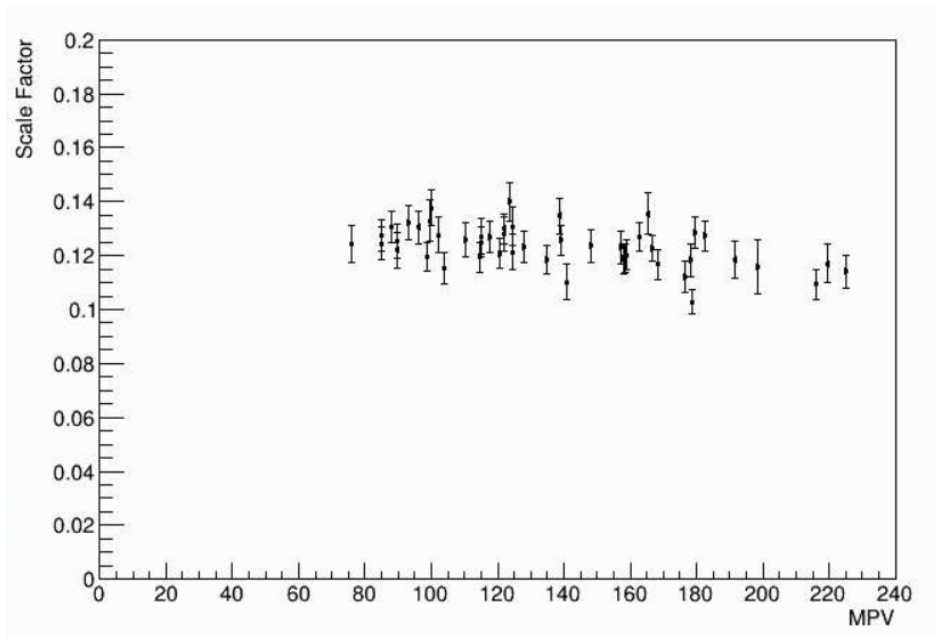

Figure 3: The measured scale factor vs MPV, showing there is little or no dependence on the MPV.

indicating that a plot of $S_{measured}$ versus MPV allows us to determine both S_{truth} and Δ^2_{LED}. As shown in Figure 3, there is no dependence on the MPV, indicating that the contribution from LED output fluctuations is much smaller than that from the number of photoelectrons, demonstrating that we do not need this more general "MPV-slope" method to determine S_{truth}.

We tested the stability of this method by looking at S values determined by different runs for the same sector. As shown in Figure 4, the scale factors for IHCal sector 19 determined from three different LED runs are consistent each other, showing the stability of the LEDs and the fitting method.
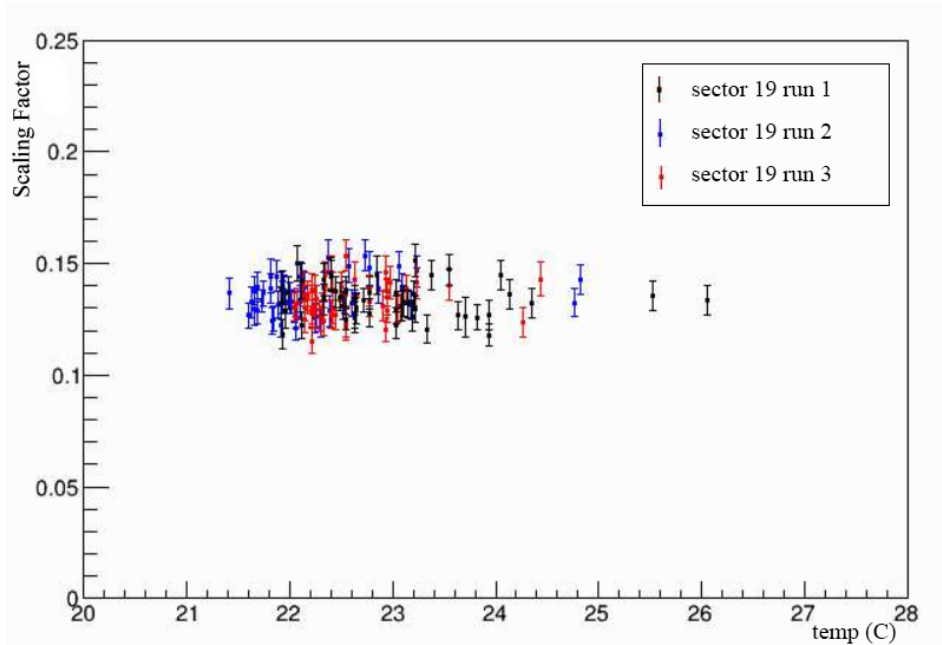
3

Figure 4: The measured scale factor vs temperature for each tower from three different LED runs for IHCal sector 19.

The results in Figure 4 are somewhat surprising, since little temperature dependence is seen in a single run over an (apparent) temperature difference as large as 4 C$^\circ$. However, S reflects the size of the current pulse produced from a single photoelectron and should be sensitive to the temperature of the SiPM because the breakdown voltage is temperature dependent. We believe the inability to see a temperature dependence in Figure 4 is due to the thermistor for each tower not necessarily measuring the temperature of the SiPM. We therefore decided to use the average temperature from all towers in each run as a proxy of the SiPM temperatures and then determine the dependence of S on the temperature.

The temperature correction constant for scale factors in IHCal and OHCal is determined using a linear fit. As shown in Figure 5, OHCal sectors gives $2.46 \pm 0.08\%$ per degree change, IHCal sectors gives $1.95 \pm 0.11\%$ per degree change away from 26 C$^\circ$.
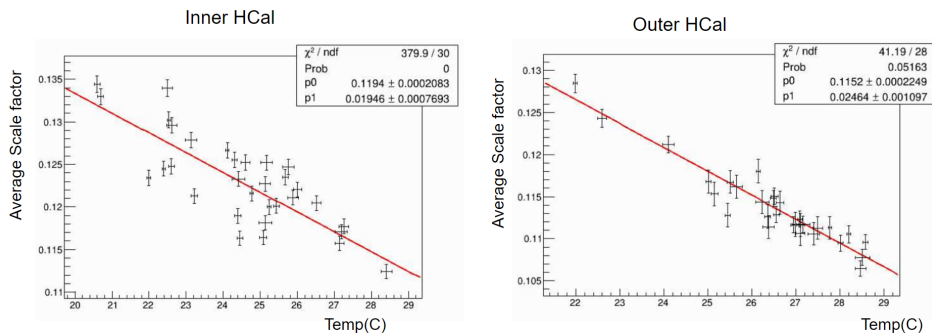

Figure 5: mean scale factor vs. mean temperature for IHCal and OHCal, p1 is the ratio of change per degree away from 26 C$^\circ$.

With the coefficients obtained from the fit, we corrected the measured scale factors back to their predicted value at 26 C$^\circ$. As shown in figure 6, the mean scale factors for each sector are consistent with each other. Also since the LED data we used to measure the scale factor is taken in low gain mode, the scale factors in figure 6 correspond to roughly 4 ADC counts per single photoelectron in

4

high gain mode, which is about 80% of the scale factor set in the simulation. We believe that could possibly be one major source of the absolute scale discrepancy mentioned in section 2.2.
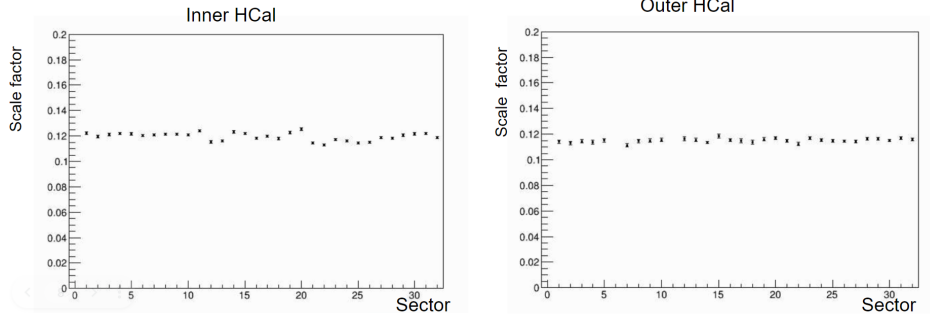

Figure 6: The average scale factor at low gain mode for each sector. Derived from the data using HBD electronics.
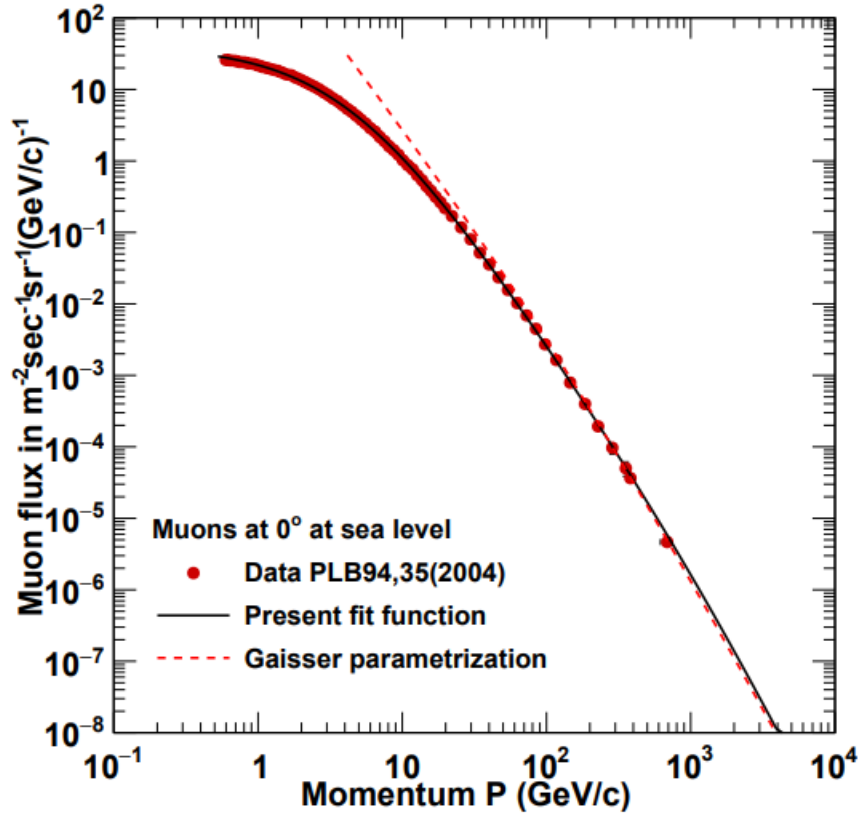
3   Rate Calculation

Figure 7: Muon momentum distribution at zenith angle = 0(red dots), fit with the parameterized function shown in [2](solid black line).

The cosmic muon rate, energy and angle distribution at sea level are well determined. As shown in Figure 7, the muon momentum distribution is well described by the function:

$$I(E, \theta = 0) = I_0 \, N \, (E_0 + E)^{-n} \left(1 + \frac{E}{\epsilon}\right)^{-1} \tag{1}$$

where E is the muon energy, I_0, E_0, n, and ϵ are parameters determined in [2], and the normalization factor $N = (n-1)(E_0 + E_c)^{n-1}$ is specified in terms of E_c, the energy cut-off of the data.
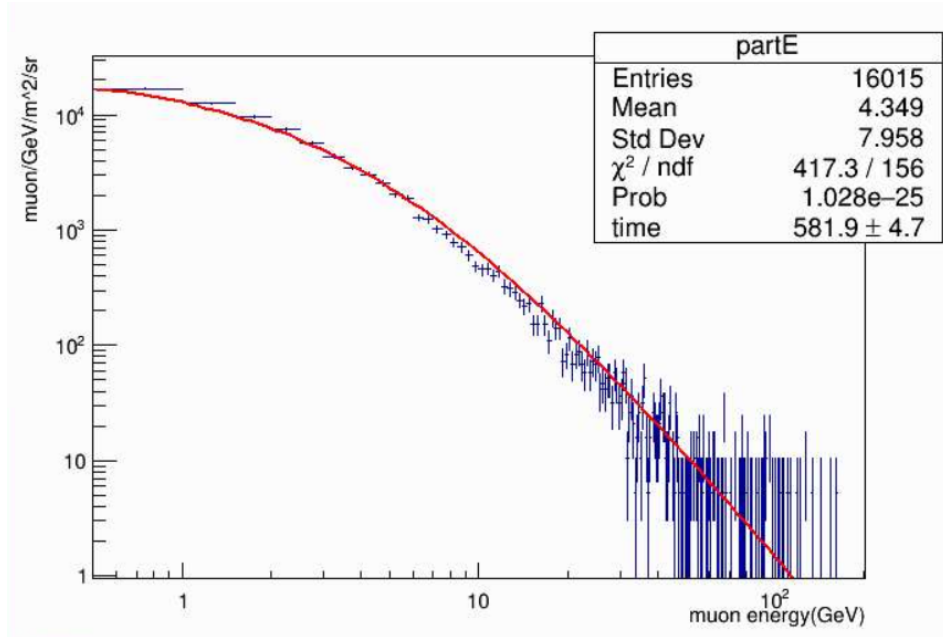

Figure 8: Generated muon energy distribution with zenith angle $< 10°$, fitted by equation 1 multiplied with one constant parameter with all other parameters fixed.

Then, to determine the time corresponding to certain number of real-world muon events, the muon energy distribution from the generator is fit using Equation 1 multiplied by one overall scaling parameter. For example, as shown in Figure 8, the energy distribution of 4 million muons generated with a $R = 6.5$m half-sphere is well fit by Equation 1, and the scaling parameter determined from the fit is the time (in seconds) required for 4M muons to be incident over the surface of the the half-sphere.
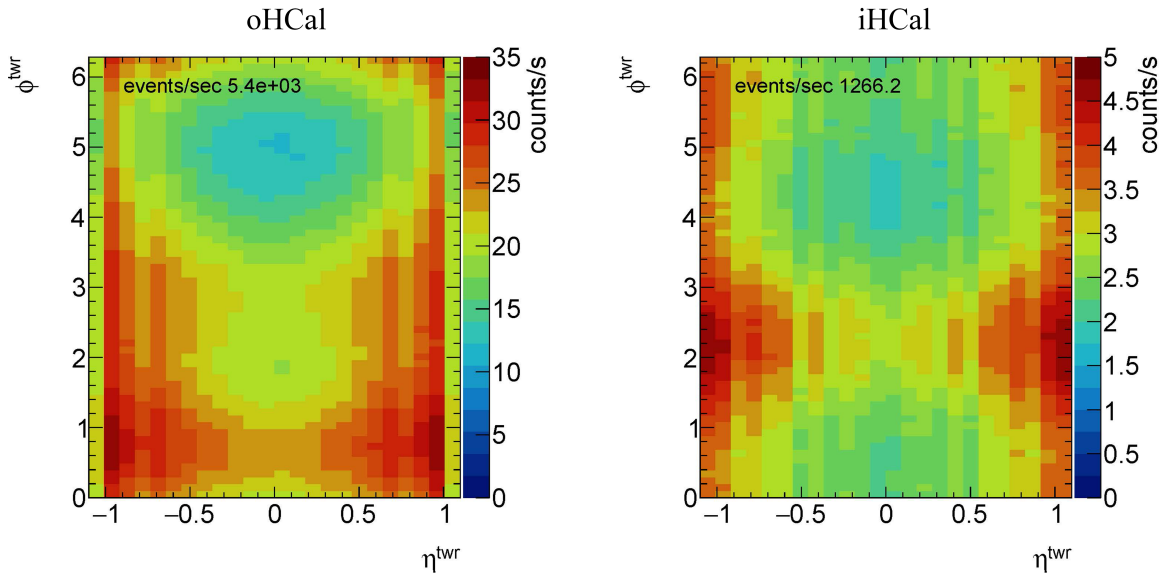

Figure 9: The rate of muon hits at each tower for oHCal(left) and iHCal(right).

6

Knowing the rate for the generated muon event, the hit rate in each tower can be determined. A hit is defined for a tower to have energy larger than 6 ADC counts for OHCal, 4 ADC for IHCal. As shown in Figure 9, the rate for the OHCal is 5.4 kHz while for the IHCal the corresponding rate is 1.2 kHz.

4 Event Selection

Of greater interest than the overall muon flux is the rate of "good" muon events that contribute to a well-defined MIP peak in each tower. The cuts used in this study, as shown in figure 10, select muon events that are perpendicular to the scintillating tiles and pass through the tower of interest entirely. The cut requires towers that are at the same η index and ± 1 ϕ index from the tower of interest have greater than 20 simulated ADC counts for the OHCal (10 counts for IHCal). The cut also requires towers that are at ± 1 η index from the tower of interest to have no more than 6 ADC counts for OHCal (4 counts for IHCal). As shown in Figure 11, the good muon rate that gives a well-defined MIP peaks[3] in the OHCal towers ranges from $0.3 \sim 3$ Hz. The ϕ dependence of the rate comes from the fact that the cut is selecting muons that are roughly perpendicular to the scintillating tiles, which for towers around $\phi = \pi/2$ (top of the barrel) and $\phi = 3\pi/2$ (bottom of the barrel) requires near-horizontal incident muon angles, which of course have a much lower rate than for near-vertical muons. For IHCal, the good muon rate is much lower due to the smaller tower size. Nonetheless, the tower energy distribution after the cuts still gives a clear MIP peak, with the good muon rates per tower range from $0.03 \sim 0.3$Hz.
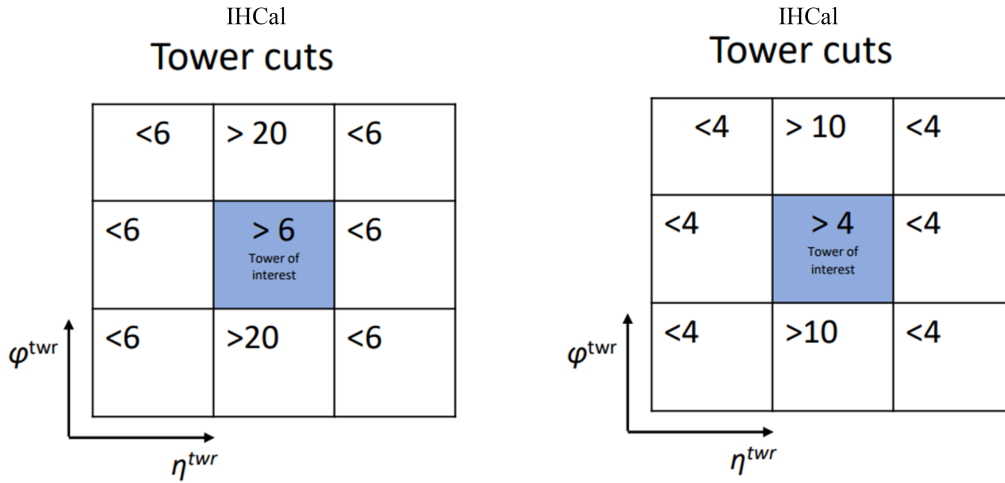

Figure 10: MIP cuts for OHCal(left) and IHCal(right), requiring muon events pass through the tower of interest entirely, perpendicular to the scintillating tiles.

Overall, these rates indicate that cosmic ray muons can provide a useful calibration tool for the HCal. Taking as a baseline the worst case rate for the top and bottom IHCal sectors of ~ 0.03 Hz $\Rightarrow \sim 100$ per hour, we see that even for this extreme case a useful MIP calibration peak can be developed in a 12-24 hours. For all other cases, the rates are 1-3 orders of magnitude larger.

---

[3]In the simulation the HCal is set to the low gain mode, need to scale up with the high gain/low gain factors if you want to compare to the cosmic testing result at 912.
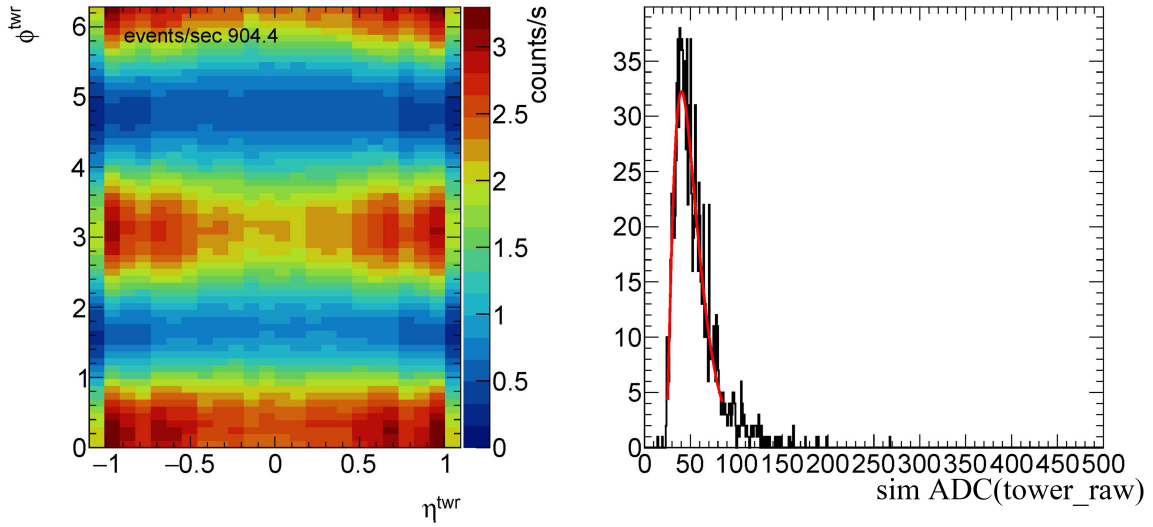
Figure 11: The rate of muon hits per tower that pass the cut for OHCal (left) and the energy deposition from one tower given by the cut fit with a gamma function (right).
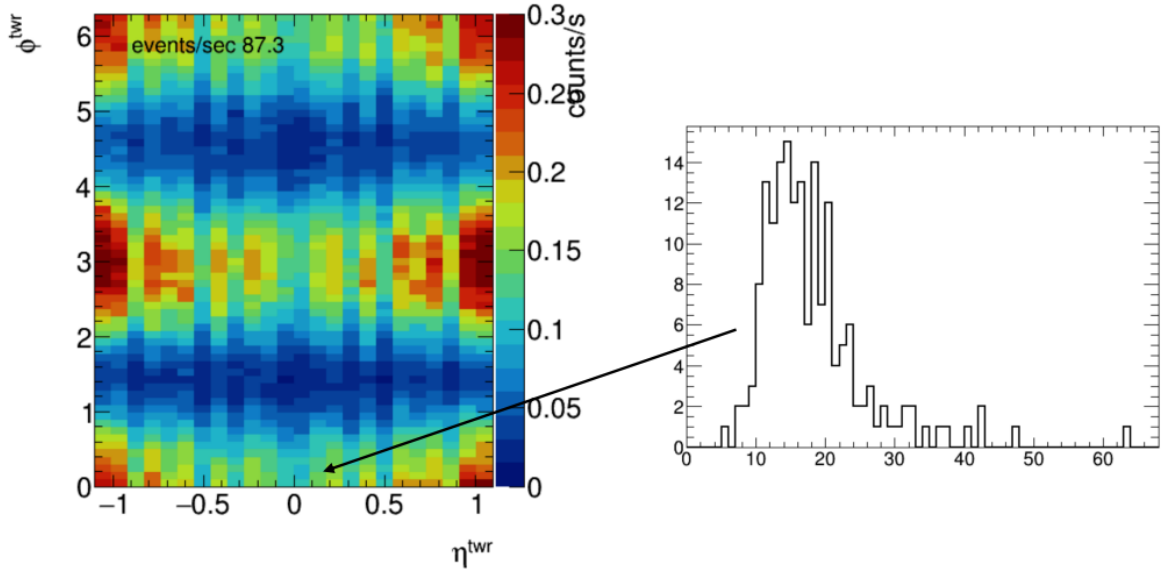

Figure 12: The rate of muon hits per tower that pass the cut for IHCal (left) and the energy deposition from one tower given by the cut (right).

5 Future Work

The results reported here were done with the previous "homogeneous" description of the HCal. We plan to go through the same procedure with the new GEANT4 setup which has a much more realistic description of the HCal. Further work should be done to study a single OHCal/IHCal sector in the simulation and compare the rate and energy distribution to the cosmic testing result. Moreover, further study of the MIP peak position determination process(fitting) needs to be done. Finally, the possibility of using less stringent cuts to simply develop profile histograms for the towers with low rates should be studied; it may be that such an approach could provide muon calibrations in less time than by

requiring a well-defined MIP peak.

Appendix1: Derivation of the Calibration Factors

Here we document our understanding of where and how the calibration factors mentioned in Section 2.1 are derived.

First, the difference between High Gain (HG) and Low Gain (LG) modes for the EMCal and the HCal is a factor of two:

$$\left.\frac{\text{HG}}{\text{LG}}\right|_{HCal} = \frac{32}{1} \quad , \quad \left.\frac{\text{HG}}{\text{LG}}\right|_{EMCal} = \frac{32}{2} = 16 \quad .$$

This was documented in an email exchange on sphenix-hcal-l on the 19th and 20th of January, 2022. between Stephan Bathe, Steve Boose and Craig Woody. It is not clear that this is relevant to the purely HCal discussion below, but factors of 16 and 32 appear in what follows, so beware. Regarding the factor of 2 that appears in the denominator of the EmCal expression, Steve Boose writes *"Sorry, I should have also pointed out that in EmCal the normal gain ¿ channel is 2, so the ratio is 16 as Craig said"*, (here "normal gain" refers to low gain). This is contrast to the HCal, where Steve describes the normal (low) gain channel as being a (unit gain) "buffer".

Second, we assume that the calibrations used in the HCal simulations are based on the observation that for some SiPM somewhere it was observed that in HG mode, the 1 photo-electron (p.e.) peak appeared in ADC Channel #5, that is

$$1 \text{ p.e.} \leftrightarrow \text{ADC Channel \#5 (HG)}$$

. This is consistent with comments on line 395ff in `Fun4All_G4_Prototype3.C`:

```
//    HCALIN:
//        1/5 pixel / HG ADC channel
//        32/5 pixel / LG ADC channel
//        0.4 MeV/ LG ADC
//        0.4/32 MeV/ HG ADC
//
//    HCALOUT:
//        1/5 pixel / HG ADC channel
//        16/5 pixel / LG ADC channel
//        0.2 MeV/ LG ADC
//        0.2/16 MeV/ HG ADC
```

Tabulating what we see in various places in the code, we can determine the inferred response in photoelectrons (N_{pe}) for a given energy deposited in the scintillator E_{dep}^{scint} in GeV:

HCal Simulation Parameters		
OHCal	Method used, comments	iHCal
`G4_HCalOut_ref.C`		`G4_HCalOut_ref.C`
High Gain = x16		High Gain = x32
16 / 5	`TowerDigitizer->set_photonelec_ADC` $(= N_{pe}/(\text{ADC Count})$ in LG mode$)$ Why different between OHCal and iHCal ??	32 / 5
16 / 5 / 0.2e-3 $\Rightarrow$ 0.4 MeV $= \frac{32}{5} N_{pe}'s$	`TowerDigitizer->` `set_photonelec_yield_visible_GeV` $(= N_{pe}'s/E_{dep}^{scint}$ in LG mode$)$	32 / 5 / 0.4e-3 $\Rightarrow$ 0.4 MeV $= \frac{32}{5} N_{pe}'s$
$\Rightarrow$ 1.0 MeV $= 16 N_{pe}'s$	Note both expressions give, same photoelectrons per GeV	$\Rightarrow$ 1.0 MeV $= 16 N_{pe}'s$

Appendix2: Code

Some code used in this analysis are listed here:

https://github.com/Shuonli/Cosmicmuongen_macro

https://github.com/bseidlit/hcalFullSim/tree/main/triggerAna

References

[1] D. Pagano et al. "EcoMug: An Efficient COsmic MUon Generator for cosmic-ray muon applications". In: *Nuclear Instruments and Methods in Physics Research Section A: Accelerators, Spectrometers, Detectors and Associated Equipment* 1014 (2021), p. 165732. ISSN: 0168-9002. DOI: https://doi.org/10.1016/j.nima.2021.165732. URL: https://www.sciencedirect.com/science/article/pii/S0168900221007178.

[2] Prashant Shukla and Sundaresh Sankrith. *Energy and angular distributions of atmospheric muons at the Earth.* 2016. DOI: 10.48550/ARXIV.1606.06907. URL: https://arxiv.org/abs/1606.06907.